Journal Pre-proof

Enhancing the Photothermal Properties of Indocyanine Green in Melanoma Spheroids via Encapsulation in Span80-Containing Lipid Nanocapsules

Siyang Wu , Taher Hatahet , Wafa Al-Jamal

PII: S0928-0987(25)00048-X
DOI: https://doi.org/10.1016/j.ejps.2025.107049
Reference: PHASCI 107049

To appear in: *European Journal of Pharmaceutical Sciences*

Received date: 8 December 2024
Revised date: 25 January 2025
Accepted date: 21 February 2025

Please cite this article as: Siyang Wu , Taher Hatahet , Wafa Al-Jamal , Enhancing the Photothermal Properties of Indocyanine Green in Melanoma Spheroids via Encapsulation in Span80-Containing Lipid Nanocapsules, *European Journal of Pharmaceutical Sciences* (2025), doi: https://doi.org/10.1016/j.ejps.2025.107049

Enhancing the Photothermal Properties of Indocyanine Green in Melanoma Spheroids via Encapsulation in Span80-Containing Lipid Nanocapsules

Siyang Wu[a†], Taher Hatahet[a,b†*], Wafa Al-Jamal[a*]

[a] School of Pharmacy, Queens University Belfast, Belfast, BT9 7BL, UK

[b] China Medical University and Queen's University Joint College, Shenyang, People's Republic of China

† Equal author contribution

*Corresponding Author:
Prof. Wafa Al-Jamal
School of Pharmacy
Queens University Belfast
MBC Building
97 Lisburn Road
Belfast
BT9 7BL
Email: w.al-jamal@qub.ac.uk
Phone: +44 (0)28 9097 2609.

Taher Hatahet
School of Pharmacy
Queens University Belfast
MBC Building
97 Lisburn Road
Belfast
BT9 7BL
Email: T.Hatahet@qub.ac.uk
Phone: +44 (0)28 9097 5732

Abstract

Indocyanine green (ICG), a well-known photosensitiser, has shown potential in photothermal therapy (PTT) for cancer treatment, but its effectiveness is limited by poor skin penetration and rapid clearance. To address this, lipid nanocapsules (LNCs) were used as nanocarriers to enhance ICG's cellular uptake and photothermal (PT) performance in melanoma cells. Utilising our recently developed Span 80-modified LNCs (LNC100-S8) with high biocompatibility and enhanced cellular uptake in B16F10 melanoma cells, ICG was loaded into LNC100-S8 using the phase inversion temperature method. The results showed that ICG encapsulation at 4.5 mg/mL maintained LNC sizes (95-105 nm). Moreover, the heating capacity of ICG in LNCs was approximately 1.5 times higher than free ICG, achieving temperature increases over 10 °C post-irradiation. In cell cancer monolayers, LNC100-S8 enhanced ICG uptake by 1.5 times compared to free ICG and reduced cell viability to 50% following 808 nm laser irradiation. More promisingly, ICG-LNC100-S8 combined with laser irradiation significantly reduced three-dimensional B16F10 spheroids size up to 11 days post-treatment compared to free ICG. Overall, our findings validate LNC100-S8, as promising nanocarriers for enhancing ICG-based PTT, supporting their potential applications *in vivo* to treat melanoma and other skin cancers.

Graphical Abstract

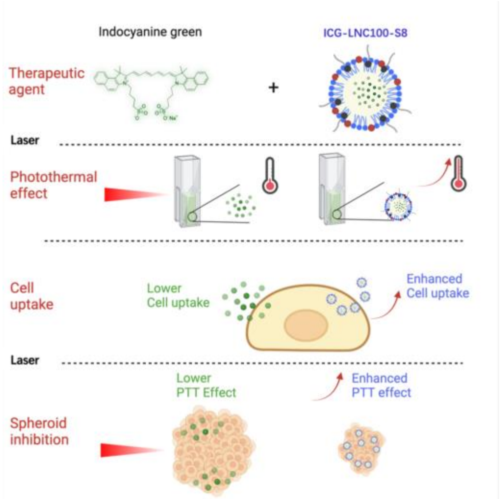

Keywords: Indocyanine Green, Lipid Nanocapsules, Span80, Photothermal Therapy, Skin Cancer, Melanoma

1. Introduction

Photothermal therapy (PTT) is a minimally invasive approach used to ablate tumours by converting light energy into heat, leading to localised hyperthermia and subsequent tumour cell apoptosis and necrosis (Chen et al., 2016; Shiyi Zhou, 2020). Compared to traditional cancer treatment modalities, such as chemotherapy or surgery, PTT is minimally invasive and has fewer side effects (Yaseen et al., 2007). PTT involves introducing a photosensitiser into the body, followed by laser irradiation to achieve the optimal temperature increase for tumour cell ablation (Lopes et al., 2022; Shiyi Zhou, 2020). Near-infrared (NIR) irradiation is advantageous for PTT, as NIR light penetrates deeper into tissues, allowing for more effective and localised tumour ablation (Liang et al., 2021). NIR-induced PTT using the non-invasive delivery of a photosensitiser holds great promise for patients with inoperable topical and near-topical cancers (Totonchy & Leffell, 2017).

Indocyanine green (ICG), is a fluorescent dye approved by the U.S. Food and Drug Administration (FDA) for angiography and lymph node biopsy. Preclinically, it has gained attention for its potential in PTT (Ntziachristos et al., 2000). ICG effectively converts light into thermal energy when exposed to NIR irradiation, making it a key component in laser-mediated PTT (Shirata et al., 2017; Zheng et al., 2011). Once delivered to the tumour site, ICG is exposed to NIR light, generating cytotoxic heat that ablates cancer cells highlighting its potential for treating topical cancers in delicate regions, such as the face or near nerves and blood vessels (Totonchy & Leffell, 2017; Yoon et al., 2017; Yorozu et al., 2022). Apart from cancer, ICG showed potential in phototherapy to treat superficial acne vulgaris with no skin irritation following ICG application to the face and the back (Genina et al., 2004). ICG also has shown a skin rejuvenation effect *in vivo* with significant improvements in wrinkles, pores, and hyperpigmentation (Jung et al., 2024). All of these reports make ICG not only a potential photosensitiser but also a skin-friendly agent (Topaloğlu et al., 2020). However, to overcome ICG degradation, and thermal instability, and improve its skin penetration (Jung et al., 2018), ICG encapsulation in skin compatible drug delivery system can open the door for ICG repurposing as a photothermal agent to treat skin cancers, such as basal cell carcinoma and melanoma.

Lipid nanocapsules (LNCs) are a promising drug delivery system due to their unique physicochemical properties, which enable efficient drug encapsulation and release (Huynh et al., 2009). LNCs consist of an oily core, a non-ionic surfactant shell and an aqueous continuous phase. They can encapsulate both hydrophobic and amphiphilic drugs (Hoarau et al., 2004). The shell of LNCs is composed of biocompatible and biodegradable excipients, such as the non-ionic surfactant Kolliphor HS15 and the amphiphilic co-surfactant phospholipids. The oil core is composed of caprylic/capric triglyceride (Labrafac), a key component that enhances lipophilic drug delivery by providing a solubilising medium for hydrophobic drugs (Idlas et al., 2021). LNCs are highly suitable for transdermal applications due to their small particle size (20–100 nm), high encapsulation for hydrophobic and amphiphilic drugs and long-term stability (Dabholkar et al., 2021). Moreover, LNCs have been shown to be more suitable for transdermal applications than other nanocarriers, such as nanocrystals (Hatahet et al., 2018). The ability of LNCs to facilitate deeper penetration into the skin is particularly advantageous for photothermal therapy (PTT), ensuring sufficient concentrations of the photosensitiser, such as ICG, at the tumour site for effective tumour ablation.

Recently, our group has recently developed Span 80-modified LNCs (LNC100-S8) with high safety in melanoma cell lines (Wu et al., 2025). We showed that a partial replacement of Kolliphor HS15 with Span 80 (35% Span 80 with 65% Kolliphor HS15 as surfactant) reduced the *in vitro* cytotoxicity on B16F10 cells compared to conventional LNC100-0 (100% Kolliphor HS15), while improving their cellular uptake (Wu et al., 2025). In the current study, we further investigated LNC100-S8 as a nanocarrier for ICG delivery and assessed their physicochemical properties and heating capacity in solution. Then, ICG-LNC100-S8 cell uptake was assessed in the B16F10 cell line, and their photothermal effect was evaluated in 2D and 3D cell models. Promisingly, our findings confirmed the successful loading of ICG into LNC-100-S8 to enhance ICG thermal properties, resulting in superior cell killing in B16F10 melanoma cells and spheroids. The present study highlights the potential of ICG-LNC100-S8 for PTT in skin cancer, which lays the foundation for future skin permeability testing and PPT *in vivo.*

2. Method

2.1. Materials

Kolliphor® HS15 (Macrogol-15-hydroxystearate), Span80 (Sorbitan monooleate), Acetonitrile (CH_3CN), Dimethyl sulfoxide (DMSO), Sodium chloride (NaCl) and Phosphate buffered saline (PBS) tablets were purchased from Sigma-Aldrich (St. Louis, MO, USA). Lipoid S 75 (Phospholipids with 70 % phosphatidylcholine) was provided as a free sample from Lipoid GmbH (Ludwigshafen, Germany). Labrafac™ lipophile WL 1349 (Medium chain triglycerides) was obtained as a free sample from Gattefossé (Saint-Priest, France). Indocyanine Green (ICG) was purchased from AdooQ BioScience (Irvine, CA, USA). RPMI 1640 medium, Dulbecco's Modified Eagle Medium (DMEM), Fetal Bovine Serum (FBS), penicillin-streptomycin, sodium pyruvate, methylcellulose, resazurin, and trypsin-EDTA were obtained from Thermo Fisher Scientific (Waltham, MA, USA). Sheath fluid was purchased from BD FACSFlow (Franklin Lakes, NJ, USA). PD-10 column was purchased from GE Healthcare (UK).

2.2. Preparation of empty and ICG-loaded lipid nanocapsules

LNCs components were weighed using an analytical balance and mixed into 7 mL glass vials according to **Table 1**. For the preparation of ICG-loaded LNCs, 16 mg (12.8 mg/g) of ICG were weighed and added to the other components. All LNC formulations were prepared using the phase inversion temperature (PIT) method (Béatrice Heurtault, 2002). Specifically, the mixed components were first heated to 85 °C by a heating plate (STARLAB, UK) and then cooled to 55 °C with continuous stirring using magnetic bars at 500 rpm. This heating-cooling cycle was repeated three times. During the third cycle, the phase inversion zone of the system was identified as the solution became clear, and

2.75 mL of cold distilled water was added to form stable and irreversible LNC100s.

Table 1. Chemical composition of the different LNC formulations prepared in the present study.

Formulation	Composition (mg)						
	ICG	Kolliphor HS15	Span80	Lipoid S75	Labrafac	NaCl	Distilled water
LNC100-0	-	121	---	18.8	302.3	22.3	785.8
LNC100-S8	-	78.6	42.4	18.8	302.3	22.3	785.8
ICG-LNC100-0	16	121	---	18.8	302.3	22.3	785.8
ICG-LNC100-S8	16	78.6	42.4	18.8	302.3	22.3	785.8

2.3. Physicochemical characterisation of LNCs

The Zetasizer Nano ZS90 (Malvern Panalytical, Worcestershire, UK), equipped with a 4.0 mW He-Ne laser operating at 633 nm, was used to determine the Z-average diameter and polydispersity index (PdI) of LNC samples. Measurements were conducted at 90°C scattering optics. Before measurement, LNC samples were diluted 100-fold with distilled water and transferred into 1mL low-volume polystyrene cuvettes (C5416, Merck, UK). Then samples were transferred into folded capillary zeta cells (Malvern Panalytical, Worcestershire, UK), and the zeta potential was tested by Zetasizer Nano ZS90. Each sample's physiochemical characteristics were obtained by averaging three measurements. The physicochemical characteristics of each sample were determined by averaging three independent measurements.

2.4. ICG encapsulation efficiency and loading into LNCs

To purify the ICG-loaded LNC100s, a PD-10 column (Cytiva Life Sciences, UK) was used. Specifically, 1 mL of ICG-LNC100s was loaded added into the PD-10 column, and then eluted with 1 mL of PBS buffer. Purified LNC100s were collected from fractions 2-5.

The encapsulation efficiency (EE) of ICG-loaded LNC100s was determined using a FLUOstar Omega Microplate Reader (BMG Labtech, Buckinghamshire, UK) with a resolution of 1 nm by measuring the absorbance of ICG at 780 nm. To quantify the encapsulated ICG, the purified ICG-LNC100s were solubilized in acetonitrile at a 1/50 (v/v) ratio, and the ICG concentration was determined using a standard calibration curve of ICG in acetonitrile (**Figure S1**). The encapsulation efficiency was calculated by taking the percentage of the encapsulated ICG concentration to the initial ICG concentration **(Equation 1)**.

$$EE\ (\%) = \frac{Concentration\ of\ Encapsulated\ ICG}{Concentrationd\ of\ Initial\ ICG} \times 100\% \qquad \textbf{Equation (1)}$$

The ICG loading was determined by using the amount of loaded ICG divided by the total weight of excipients **(Equation 2)**.

$$ICG\ loading\ (\mathrm{w/w}\ \%)\ =\ \frac{Amount\ of\ loaded\ ICG\ (mg)}{Amount\ of\ excipients\ (2.5\ g)} \qquad \textbf{Equation (2)}$$

2.5. Heating capacity of ICG-LNC100s

Free ICG solution, ICG-LNC100-0, and ICG-LNC100-S8 were diluted in water to concentrations of 6, 12, and 24 µg/mL based on the ICG concentration. 1 mL from each sample was separately transferred into polystyrene cuvettes. The experiments were conducted under controlled laboratory conditions, with all samples maintained at a constant temperature of 25°C in the water bath (Grant, UK) at the beginning of the experiment (recorded as T_0). Near-infrared irradiation (NIR) was performed using an 808 nm wavelength laser (Optoelectronics Tech Co., LTD, PSU-W-FC, UK) with a power density of 2 W/cm^2 from a distance of 5 cm. Samples were then irradiated for 3 minutes. During irradiation, the temperature of each sample was measured and recorded every minute (T_1 to T_3) using fibre optic temperature probes (OSENSA Innovations, UK). The temperature difference was calculated by subtracting the initial temperature (25°C) from the temperature measured every minute **(Equation 3)**.

$$\Delta T = T_n - T_0 \qquad \textbf{Equation (3)}$$

Where ΔT means the change in temperature where T_n represents the temperature measured at each time point (1 to 3 minutes), and T_0 is the initial temperature before irradiation.

2.6. *In vitro* 2D cellular characterisation

2.6.1. Cell line and cell culture

Murine melanoma cell line B16F10 (CRL-6475™ ATCC®, UK) was cultured in RPMI 1640 (21875-034, Gibco) medium supplemented with 10% FBS, 1% penicillin-streptomycin and 1% sodium pyruvate. Immortalised murine stellate cell (SC) line was kindly provided by Prof. Angela Mathison (Medical College Wisconsin, USA), and cultured in Dulbecco's Modified Eagle Medium (DMEM, 41965-039, Gibco) supplemented with 10% fetal bovine serum (FBS) and 1% penicillin-streptomycin.

All cells were maintained in T-75 tissue culture flasks (Sarstedt, Germany) at 37 °C in a humidified incubator with 5% CO_2. To maintain exponential growth, cells were passaged 1 in 10 ratios, 2-3 times each week using 0.05% Trypsin-EDTA and fresh medium when they reached 80% confluence.

2.6.2. *In vitro* cellular uptake

B16F10 cells (2×10^5 cells/well) were seeded into a 12-well plate (Sarstedt, Germany) and incubated for 24 h. For the uptake studies, B16F10 cells were treated with 1 mL of ICG, ICG-LNC100-0 or ICG-LNC100-S8 at 6 µg/mL and 12 µg/mL ICG in a complete medium, and incubated for 1, 3, and 24 hours. After incubation, cells were washed three times with 1 mL sterile PBS buffer and subsequently lysed with 0.2 mL dimethyl sulfoxide (DMSO). The lysates were collected in 1.5 mL Microcentrifuge tubes (Fisher Scientific, UK), and ultrasonicated for 10 minutes in an Ultrasonicator (VWR, UK) to help mix. The absorbance of ICG in the lysates was measured at 780 nm using FLUOstar Omega Microplate Reader (BMG Labtech, UK). The data was shown as the fold change in absorbance as **equation 4**.

$$The\ fold\ change\ in\ absorbance = \frac{The\ absorbance\ of\ test\ group}{The\ absorbance\ of\ control\ group} \qquad \textbf{Equation (4)}$$

2.6.3. *In vitro* cellular toxicity and photothermal therapy effect

B16F10 cells (1.5×10^4 cells/well) were seeded into a 96-well plate (Sarstedt, Germany) and incubated for 24 hours. After incubation, the old medium was replaced with 200 µL fresh RPMI 1640 medium containing free ICG, ICG-LNC100s, empty LNC100s or 10% dimethyl sulfoxide (DMSO) as a positive control. After 3 and 24 hours of incubation, the medium was removed, and the cells were washed three times with 200 µL sterile PBS buffer then incubated with 200 µL fresh medium. Next, cells were irradiated from a 5 cm distance with laser light (808 nm, 2 W/cm²) for 3 minutes per well, then followed by resazurin assay. In the non-irradiated groups, cell viability was directly assessed. The medium was replaced with a 10% resazurin solution (0.1 mg/mL, 200 µL) and incubated for 4 hours. After incubation, 150 µL of the supernatant was transferred to a black 96-well plate, and fluorescence was measured using a FLUOstar Omega Microplate Reader with excitation/ emission at 544/590 nm respectively. One well without cells containing only 10% resazurin solution was used for blank correction. Cell viability was assessed using **equation 5**.

Equation (5):

$$Cell\ viability\ (\%) = \frac{(Fluorescence\ of\ tested\ cells - Fluorescence\ of\ blank\ correction)}{(Fluorescence\ of\ untreated\ control - Fluorescence\ of\ blank\ correction)} \times 100\%$$

2.7. *In vitro* 3D cellular characterization

2.7.1. B16F10 spheroid formation using methylcellulose

B16F10:SC (1:1) cells were dispersed in 200 µL of complete RPMI 1640 medium containing 0.24% methylcellulose and seeded at a total density of 5000 cells/well in a 96-well round-bottom plate (TC-Plate 96 Well Standard, R, UK). The medium was refreshed every 2 days by removing 100 µL of medium from each well and replacing it with 100 µL of fresh medium. Spheroids were maintained for 7 days to monitor growth. Images of spheroids were captured using a light microscope (OLYMPUS, CKX41, UK) at 10× magnification, equipped with a QImaging (MicroPublisher 3.3 camera, UK). The size of the spheroids was calculated using ImageJ software (LOCI, University of Wisconsin, US).

2.7.2. Photothermal effect in B16F10 spheroids

B16F10:imPSC2 spheroids (1:1) were cultured for 3 days until the spheroids reached an approximate diameter of 550 µm. The spheroids were then treated with free ICG or ICG-LNC100s at concentrations of 24 and 48 µg/mL for 24 hours. The cells in the negative control group were cultured with a complete medium, while the positive control group contained 10% dimethyl sulfoxide (DMSO) in the medium. On day 4, spheroids were washed gently with a sterile PBS buffer. Then fresh medium was added, and cells were irradiated with a 2 W/cm² laser at 808 nm for 5 minutes from a distance of 3 cm. Non-irradiated spheroids were washed and maintained with a fresh medium. The cells were maintained by changing the medium every 2 days. The diameter of the spheroids was monitored using the Cell3iMager neo (SCREEN Holdings Co., Ltd., UK). The size of the spheroids was calculated using ImageJ software (LOCI, University of Wisconsin, US).

2.8. Statistical analysis

Prior to statistical analyses, the mean, standard deviation, and normality distribution of all data sets were calculated. A two-tailed independent t-test was used to compare the means of the two groups. One-way analysis of variance (ANOVA) was performed to analyse differences between the means of more than two groups, followed by Tukey's Honestly Significant Difference (TukeyHSD) post-hoc test. All statistical tests were performed using GraphPad Prism 10 (GraphPad Software, Inc., USA).

3. Results

3.1. Physiochemical properties of ICG-loaded LNCs

Initially, empty conventional (LNC100-0) and Span80-modified (LNC100-S8) LNCs were prepared using the phase inversion temperature (PIT) method **(Figure 1**). Both LNCs had comparable hydrodynamic diameter and PDI of LNCs (101 ± 2 nm, 0.07 ± 0.01 vs. 94 ± 2 nm, 0.13 ± 0.05, respectively) (**Figure 1A**). Both LNCs exhibited comparable zeta potential (**Figure S2**). Similarly, loading ICG of up to 4.5 mg/mL showed comparable particle size and pdI values for LNC100-0 (103 ± 3 nm, 0.11 ± 0.01) and LNC100-S8 (105 ± 3 nm, 0.19 ± 0.03) (**Figure 1A**). Interestingly, both LNCs demonstrated comparable ICG encapsulation efficiencies (%EE) of and loading capacities (99 ± 2 %, 12.5± 4 mg/g vs. 96 ± 1 %, 12.1 ± 3 mg/g, respectively) (**Figure 1B**). Furthermore, ICG-LNCs exhibited high stability up to 14 days storage at 4°C, with minimal changes in the hydrodynamic diameter and ICG % EE (**Figure S3**).

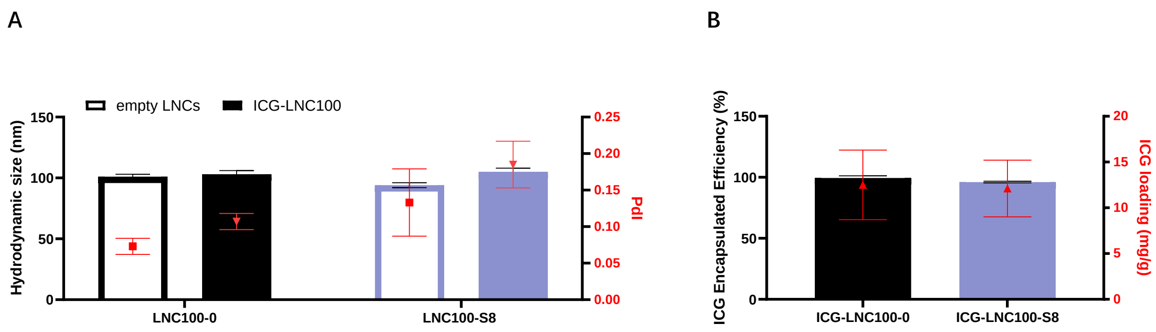

Figure 1. Physiochemical properties of ICG-loaded LNCs. 4.5mg/mL ICG was loaded into conventional (ICG-LNC100-0) and Span80-containing (ICG-LNC100-S8) LNCs. (A) Hydrodynamic size and polydispersity index (pdI), and (B) ICG encapsulation efficiency and loading capacity. LNCs were characterised by DLS and UV plate reader, respectively (n=3).

3.2. Heating capacity of ICG-loaded LNCs

To determine the heating capacity for ICG in its free or LNC-loaded form, ICG, LNC100, and ICG-LNC100-S8 samples at 6, 12 and 24 µg/mL were irradiated for 1-3 minutes with 808 nm laser at 2 W/cm². **Figure 2** shows that at all concentrations, ICG-LNCs showed a statistically higher heating capacity than free ICG solution ($p<0.005$). Furthermore, comparable heating capacity was achieved with both LNC formulations following 2- and 3-minute radiation. Nevertheless, at 1-minute irradiation, ICG-LNC100-S8 showed statistically higher heating capacity than conventional ICG-LNC100-0 with 12 and 24 µg/mL of ICG ($p < 0.05$).

After 3 minutes of irradiation, the temperature increased by 6°C, 11°C, and 19°C with 6, 12, and 24 µg/mL of free ICG solution, respectively. In parallel, ICG-LNCs exhibited significantly improved heating capacity across all concentrations with an average temperature increase of 9°C, 17°C, and 26°C at 6, 12, and 24 µg/mL respectively ($p < 0.005$).

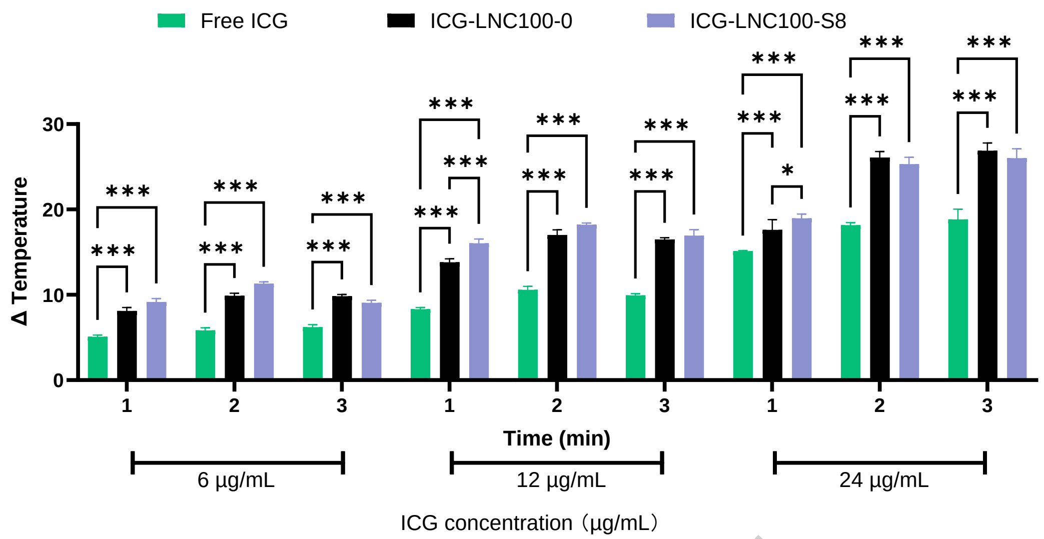

Figure 2. Heating capacity of ICG-loaded LNCs. Samples of ICG, ICG-LNC100-0 and ICG-LNC100-S8 at 6, 12, and 24 µg/mL were heated for 1-3 min with a 2 W/cm^2 laser at 808 nm from a 5 cm distance. During a 3-min heating period, the temperature of the sample was recorded every minute using an optical fibre. Statistical analysis was performed using one-way ANOVA * p< 0.05, ***p<0.005 (n=3).

3.3 Cellular uptake of ICG-LNCs in B16F10 cell lines

The cellular uptake of free ICG, ICG-LNC100-0 and ICG-LNC100-S8 was assessed in the B16F10 cell line at concentrations of 6 and 12 µg/mL (**Figure 3A and B**). At 6 µg/mL, minimal uptake was observed at 1 hour; however, a significantly higher cellular uptake was observed for ICG-LNC100-S8 than free ICG and ICG-LNC100-0 after 3 hours of incubation ($p < 0.005$). As incubation time increased to 24 hours, the cellular uptake of free ICG and ICG-LNC100-0 appeared to reach similar levels ($p > 0.05$). However, still, ICG-LNC100-S8 exhibited a significantly higher cellular uptake than ICG-LNC100-0 ($p = 0.026$) (**Figure 3A**). At 12 µg/mL, differences in cellular uptake among formulations were only observed at 3 and 24 hours. At the 3-hour time point, the cellular uptake of ICG-LNC100-S8 showed a statistical increase than free ICG and ICG-LNC100-0 ($p=0.005$ and $p=0.008$). As incubation time increased to 24 hours, the cellular uptake of ICG-LNC100-S8 was approximately 1.5 times higher than that of free ICG and ICG-LNC100-0 ($p < 0.005$) (**Figure 3B**).

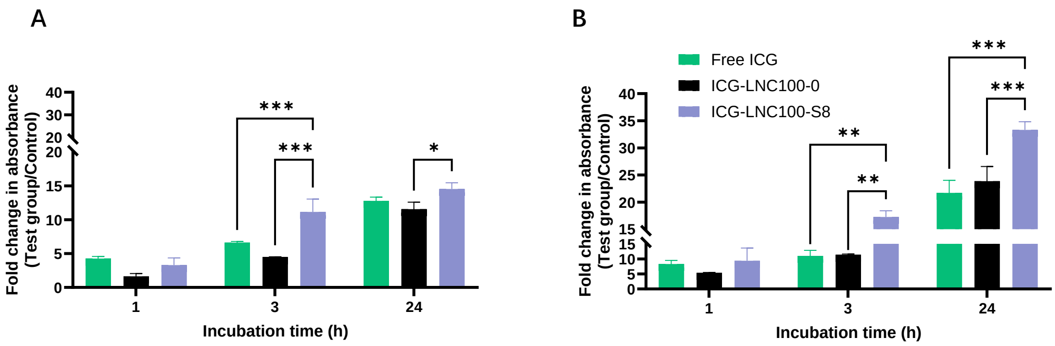

Figure 3. Cellular uptake of ICG-loaded LNCs in B16F10 cell line. Cellular uptake of free ICG, ICG-LNC100-0 and ICG-LNC100-S8 in B16F10 monolayers treated with (A) 6 µg/mL and (B) 12 µg/mL of ICG. B16F10 cells were incubated with different ICG formulations in complete RPMI1640 medium for 1, 3 and 24 hours. Cells were washed and lysed with 0.2 mL DMSO and ICG absorbance was measured using the plate reader. Statistical analysis was performed using one-way ANOVA * $p< 0.05$, ** $p< 0.01$, *** $p<0.005$ (n=3).

3.4. Photothermal effect of ICG-LNCs on B16F10 monolayers

Following the confirmation of efficient uptake of ICG-LNC100 formulations by B16F10 melanoma cells, their *in vitro* cytotoxicity and photothermal (PT) effects were investigated in the same cell line following 3 hours of incubation.

Initially, the toxicity of our empty LNC100-0 and LNC100-S8 were evaluated following 3-hour incubation with 440-1700 µg/mL of LNC concentrations that will be equivalent to ICG-loaded LNCs, containing 6-24 µg/mL of ICG. In agreement with our previous results, LNC100-S8 exhibited minimal toxicity compared to LNC100-0, where the latter showed concentration-dependent toxicity **(Figure 4A, solid bars)**. More importantly, 3-min laser irradiation did not affect the viability of cells incubated with all empty LNCs **(Figure 4A, striped bars)**. Similar biocompatibility was observed with free ICG and ICG-loaded LNCs in the absence of irradiation at 3-hour incubation (**Figure 4B, solid bars**). Nevertheless, 3-hour incubation combined with irradiation resulted in significant photothermal effects with ICG and ICG-LNCs at all concentrations ($p < 0.05$) except with ICG-LNC100-0 at 24 µg/mL, due to the inherent toxicity of ICG-LNC100-0 ($p > 0.05$) (**Figure 4B, striped bars**). The application of laser at 12 µg/mL decreased cellular viability by 20%, 23% and 25% with free ICG, ICG-LNC100-0 and ICG-LNC100-S8, respectively. The application of laser at 24 µg/mL decreased cellular viability by 36% and 42% with free ICG and ICG-LNC100-S8, respectively. It is important to note that 1-minute laser irradiation was not sufficient to induce significant cell toxicity (**Figure S4**).

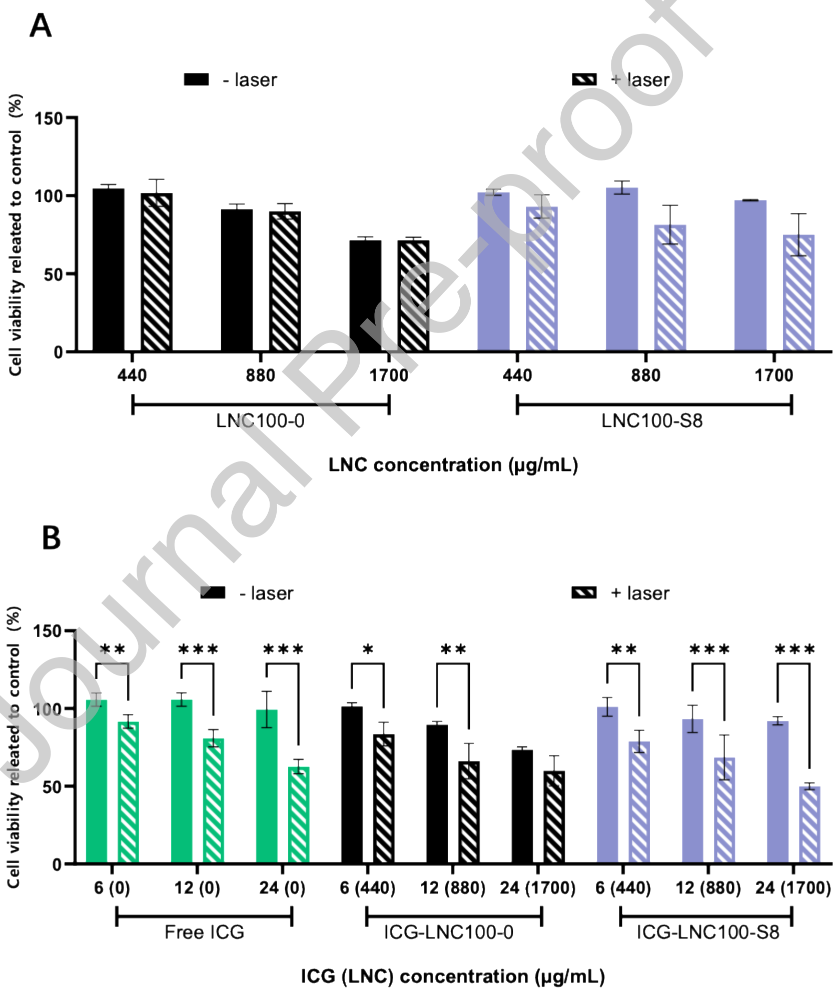

Figure 4. Photothermal effect of ICG-loaded LNCs on B16F10 melanoma cell line. Different concentrations of (A) empty LNCs or (B) ICG-LNCs and free ICG were incubated with B16F10 cell line for 3 hours. Irradiated samples were subjected to 3 min with 2W/cm^2 laser at 808 nm. Cell-viability was tested by resazurin assay (n=3, 5 wells/ condition). Statistical analysis was performed using t-test * p< 0.05, **p< 0.01, ***p<0.005.

3.5. Photothermal effect of ICG-LNCs on three-dimensional B16F10 spheroids

To evaluate the photothermal effect of our developed ICG-LNCs into a complex *in vitro* model, a three-dimensional co-culture model of B16F10: stellate cells (1:1) was successfully developed (**Figure S7)**. Next, spheroids were incubated with 48 µg/mL of ICG for 24 hours, then washed and irradiated for 5 minutes at 2 W/cm². The spheroids' diameter of the irradiated and the non-irradiated spheroids were monitored for up to 11 days. As expected, no significant inhibition of spheroid proliferation was observed in the absence of laser irradiation compared to the negative control group (**Figure 5A**). However, upon irradiation, a marked inhibition of B16F10 spheroid proliferation was observed. By day 11, a reduction of 28.3%, 24.5% and 33.7% in spheroid size was observed with free ICG, ICG-LNC100-0 and ICG-LNC100-S8, respectively, compared with the control group ($p < 0.05$) (**Figure 5B**). Promisingly, the highest spheroids inhibition was obtained with ICG-LNC100-S8, with significant differences between free ICG and ICG-LNC100-0, which could be attributed to their higher cellular uptake (**Figure 3**). It is worth mentioning that a significant spheroid inhibition was observed at 24 µg/mL of ICG, however, no significant differences were observed among the three ICG formulations (**Figure S8**).

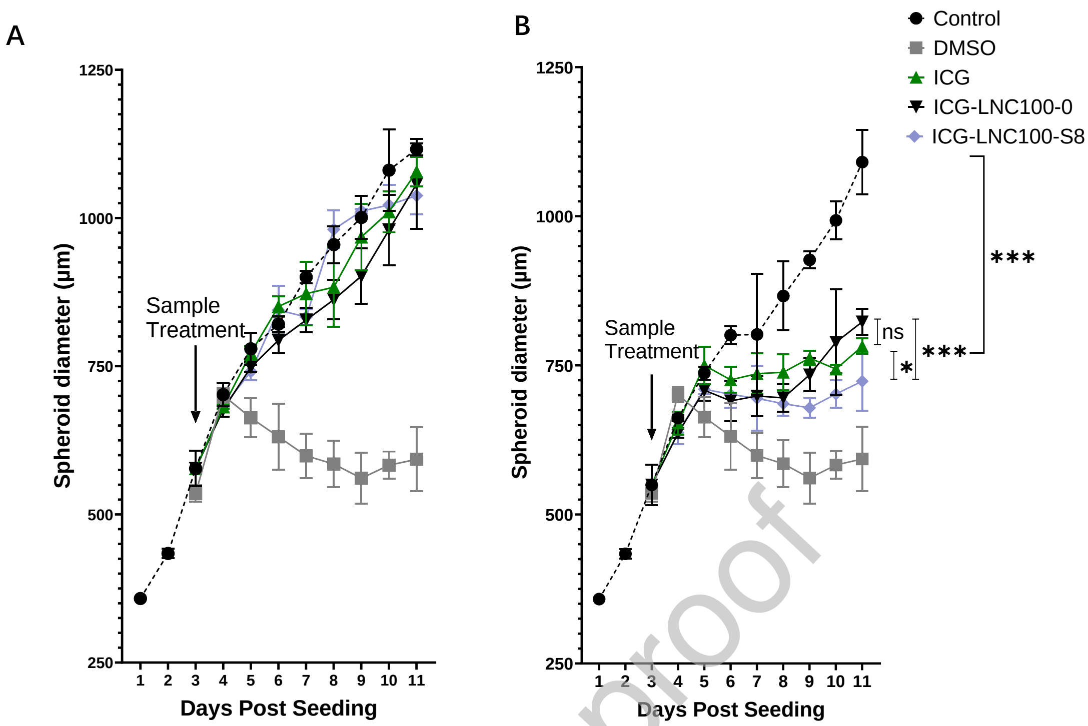

Figure 5. Photothermal effect of ICG-loaded LNCs on B16F10 co-cultured spheroids. (A) non-irradiated group, (B) irradiated group. B16F10:SC spheroids (1:1) were seeded in the 96-round bottom plate with medium containing 0.24% methylcellulose at 5000 cells/well for 3 days then treated with free ICG or ICG-LNC100-0 or ICG-LNC100-S8 at 48 µg/mL. At day 4, spheroids at the irradiated group were washed and irradiated for 5 min with 2 W/cm^2 laser at 808 nm with a distance of 3 cm. The spheroid diameter was monitored over time using the Cell3iMager neo (n=3, 6 wells/ condition). 10% DMSO was used as a positive toxicity control. Statistical analysis was performed using one-way ANOVA * p< 0.05, ***p<0.005.

4. Discussion

PTT is an interesting approach to locally treat skin with reduce side effects compared to chemotherapy (Li et al., 2020; Zhi et al., 2020). Due to its deeper penetration depth, NIR irradiation has been higher potential for clinical translation, particularly with the development of NIR photosensitisers and photothermal (PT) agents, such as ICG (Andreea Campu, 2020; Kim & Kim, 2023). ICG is a fluorescent dye that is FDA-approved in diagnostic imagining.

Moreover, ICG is capable of converting NIR energy into thermal energy capable of cancer ablation (Jian et al., 2015; Sevieri et al., 2020; Yoon et al., 2017). However, the direct application of free ICG solution to skin cancer is challenged by its low skin penetration.

LNCs have been extensively investigated in drug delivery to skin tissue (Abdel-Mottaleb et al., 2011; Elmowafy et al., 2022; Hatahet et al., 2018; Lee et al., 2019; Shiyi Zhou, 2020). They have the potential to be commercialised in the cosmetic field. LNCs have been used to deliver ingredients like quercetin, coenzyme Q10, and retinyl palmitate to the skin (Hatahet et al., 2017; Nguyen et al., 2016; Simon et al., 2020; Terroso et al., 2009). Furthermore, LNCs exhibit high stability. For instance, LNC100 loaded with benznidazole maintained physical stability for up to one year when stored at 4 °C (Arrua et al., 2023). Similarly, curcumin-loaded LNCs prepared by comparable methods showed stable encapsulation efficiency over 30 days under 4 °C storage conditions (Mazzarino et al., 2010). Furthermore, storage under light-protected conditions is likely to be effective in preserving the stability of light-sensitive drugs encapsulated in LNCs (Mazzarino et al., 2010). They enhance penetration and provide a controlled release for prolonged activity, particularly for anti-ageing and skin-brightening products. However, no studies have explored LNCs in delivering PT agents for skin cancer. Recently, our group has developed a Span80-modified LNC formulation (LNC100-S8) and showed its reduced toxicity and enhanced cellular uptake in B16F10 melanoma cell lines (Wu et al., 2025), which could have a huge promise for improving ICG photothermal efficacy in skin cancer. Our developed ICG-LNCs, can be directly applied to the skin surface or extended to other topical formulations, such as gels or microneedles, to leverage their small size and skin penetration capabilities for treating superficial skin cancers (Abd-El-Azim et al., 2022; Cordeiro Lima Fernandes et al., 2021; DeMuth et al., 2012; El-Sheridy et al., 2019). Alternatively, for deeper tumours or more targeted therapies, injection can provide better localisation and therapeutic efficacy (Hureaux et al., 2010; Morille et al., 2011).

The use of the Phase Inversion Temperature (PIT) method in this study proved effective in producing lipid nanocapsules with high encapsulation efficiency and stability under laboratory conditions (Heurtault et al., 2002). The process is relatively simple, energy-efficient, and holds potential for industrial applications (Dabholkar et al., 2021; Huynh et al., 2009). To the best of our knowledge, this is the first report of ICG-loaded LNCs with a high ICG loading of 12.3 mg/g (4.5 mg/mL) (**Figure 1**) with good stability up to 14 days (**Figure S3**). Our ICG-LNCs exhibit a 10-fold increase compared to ICG liposomal formulation that loaded 350-430 µg/mL (Shemesh et al., 2014) and a 15-fold increase compared to the 300 µg/mL loaded in lipid-polymer nanoparticles (Zhao et al., 2014). The higher loading capacity of LNCs might be explained by the contribution of both the hydrophobic core and the hydrophilic shell in ICG loading. Hsu et al. (2020) showed a significant difference in ICG encapsulation efficiency when loading into nanoparticles composed of a hydrophobic hybrid chitosan/DBA core and nanoparticles made without the hydrophobic core. The drug loading percentage increased from 2.0 ± 0.1% to 3.3 ± 0.2% compared to particles made without the hydrophobic core. They believed that hydrophobic interaction provided by DBA plays a key role in improving the drug loading percentage of ICG (Hsu et al., 2020). These results indicate that ICG-LNCs were successfully formulated with high drug loading that matches the 5 mg/mL of ICG used in clinical applications (Muraleedharan & Tripathy, 2023; Shirata et al., 2017; Teng et al., 2021).

The ability of ICG and ICG-LNCs to induce heat was assessed in an aqueous environment (**Figure 2**). Our findings confirmed that the photothermal effect of ICG solution and ICG-LNCs was concentration-dependent (Lee, 2021). More importantly, ICG-LNCs significantly enhanced ICG heating capacity (**Figure 2**).

For instance, following 3-minute irradiation at 24 µg/mL ICG, the changes in temperature increase were 19 ± 1 °C, 27 ± 1 °C and 26 ± 1 °C with free ICG, ICG-LNC100-0 and ICG-LNC100-S8, respectively. At concentrations of 12 and 24 µg/mL, ICG-LNCs consistently reached temperatures above 45 °C, meeting the effective “hyperthermia range” of 42–47 °C required for tumour ablation (Pereira Gomes et al., 2019). Zheng *et al* reported a similar enhancement in heating capacity with ICG-loaded nanoparticles, where ICG-PL-PEG nanoparticles showed a 1.3-fold higher temperature than free ICG under similar heating conditions. (Zheng et al., 2012). Using polymeric nanomicelles, the enhancement of the PT effect of ICG was also demonstrated in HeLa cells (Jian et al., 2015).

LNCs are known to be toxic to 2D cell cultures due to their high concentration of surfactants (Maupas et al., 2011). Tackling this issue, our group illustrated the impotence of the surfactant selection to increase LNCs biocompatibility in melanoma cells, where incorporating 35% of span 80 into the conventional LNCs improved their compatibility (Wu et al., 2025). Accordingly, both empty LNC100-S8 and ICG-LNC100-S8 demonstrated lower cytotoxicity than their empty or ICG-LNC100-0 counterpart under the same incubation conditions without laser irradiation (**Figure 4**). Furthermore, LNC100-S8 exhibited a 1.43 times higher uptake compared to LNC100-0 and a 1.67 times higher uptake than free ICG in B16F10 melanoma cells (**Figure 3**). These findings are consistent with our previous results using Dil-labelled LNCs (Wu et al., 2025). Promisingly, the safer ICG-LNC100-S8 with its higher cellular uptake exhibited significant PT effects under laser irradiation, resulting in approximately 30% reductions in cell viability compared with the non-laser group, something not visible with ICG-LNC100-0 (**Figure 4B**). The PT effect was more pronounced with higher ICG concentrations, indicating a dose-dependent response. Similar findings were reported in previous studies with SKOV3 cells (human ovarian cancer cell line), where PT efficiency increased with increasing ICG concentrations from 0.5 to 50 µg/mL (Li et al., 2017). Overall, LNC100-S8 is a safer and more effective delivery approach for ICG over conventional LNC100-0 in 2D cell culture melanoma model.

Unlike monolayer, 3D cell culture models can offer an advanced level of cellular interaction and polarity, thus better mimicking the *in vivo* conditions. Spheroid models more accurately represent tumour behaviour by simulating gradients of oxygen, nutrients, and drug penetration, factors that critically impact treatment efficacy (Abbas et al., 2023). To establish a 3D model of B16F10 spheroids, various methods were tested. Initially, 3D spheroids were attempted using 1-2 × 10^4 cells/well seeded in using agarose-coated 96-well plates to form regular spheroids according to Mu et al. (2021). However, although the cells aggregated, our cells failed to form homogenous spheroids after 10 days in culture (**Figure S5**). Given the challenges with the agar-coated method, the hanging drop method was also employed, with 5,000 cells/drop seeded on the lid of a petri dish in a complete cell culture medium, which was reported to form spheroids within 7 days (Filipiak-Duliban et al., 2022). Similarly, we had similar difficulties with the hanging-drop method, as spheroid formation could not be reproduced. While B16F10 cells initially formed aggregates in the hanging droplets, these aggregates failed to develop into spheroids after transfer between plates (**Figure S6**). To address these issues, we developed a co-culture method using a 1:1 ratio of B16F10 and stellate cells with media containing 0.24% methylcellulose and starting with 5000 cells/well of 96-well-plate, resulting in regular-shaped spheroids that remained stable over time (**Figure S7**). Over the 7-day observation period, the spheroids exhibited consistent growth and maintained a uniform spherical shape. Promisingly, our co-culture model better mimics the tumour microenvironment, where stromal cells play a critical role in tumour development and therapy resistance (Sharma et al., 2024).

Interestingly, irradiated B16F10 spheroids treated with ICG-LNC100-S8 exhibited up to a 34% reduction in size, significantly more than the reductions observed with free ICG (28%, $p < 0.05$) and ICG-LNC100-0 (24%, $p < 0.005$) (**Figure 5B**). The superiority of ICG-LNC100-S8 over free ICG was not observed in the 2D experiments (**Figure 4B**). Compared to traditional 2D monolayer cultures, which allow uniform exposure to treatments, the 3D model introduces barriers to drug penetration, closely simulating the challenges faced when treating tumours in patients (Abbas et al., 2023). This is the first study to demonstrate that lipid nanocapsules can effectively enhance the PT effect of ICG in a 3D B16F10 model. Previously, Li et al. (2017)reported that, free ICG reduced SKOV3 spheroid diameter by 21.5%, while ICG-PEI-HAuNS achieved a 50.2% reduction after 5 days of laser irradiation. The significant reduction in spheroid size achieved with ICG-LNCs suggests that these formulations effectively overcome the delivery and penetration barriers that commonly hinders solid tumour treatment, which requires further investigations. Moreover, the tailored composition of LNC100-S8 to reduce LNCs inherent toxicity and increase LNCs uptake by B16F10 significantly improved the PT effect compared to conventional LNC100-0 ($p < 0.05$) (**Figure 5B**). More promisingly, LNCs have shown to reduce the secretion of tumour growth factors and thus control tumour growth in both B16F10 (mouse melanoma) and SK-Mel-28 (human melanoma) cells due to their supramolecular structure (Drewes et al., 2017). Collectively, all the factors could have enhanced the ICG-LNC100-S8 PT effect; however, the exact mechanism is yet to be elucidated.

This study also highlighted the need to appropriately use cell culture model in understanding LNCs cytotoxicity. In the 2D model of this study, empty LNC100-0 reduced cell viability by 30-50% (**Figure 4A**), whereas in the 3D model, it had almost no effect on spheroid growth (**Figure 5A**). This finding can be explained by the difference in resistance of 2D and 3D cell models to nanoparticles (Zuchowska et al., 2017). According to Gonçalves et al. (2017) glioblastoma multiforme (GMB) spheroids were more resistant to drugs and other therapies than monolayer cells. The 3D models were shown to have higher photothermal tolerance than 2D models, and the cell viabilities of cells in 3D models after NesPEG-AuNR/laser treatment was 26% higher than that in 2D models (Gonçalves et al., 2017). These findings emphasize the critical importance of 3D models for accurately assessing both the therapeutic efficacy and cytotoxicity of nanoparticle-based treatments.

5. Conclusions

In this study, we successfully loaded ICG into LNCs with high loading efficiency. Our work confirmed the ability of LNCs to enhance the PT effect of ICG in both 2D and 3D models of B16F10 melanoma cells. The results demonstrated that ICG loaded into Span-80 modified LNCs significantly improved the cellular uptake of ICG with minimal cytotoxicity. Consequently, LNC100-S8 enhanced the ICG photothermal effect and exhibited statistically superior efficacy, compared to ICG, in inhibiting spheroid proliferation in the 3D co-culture model. Overall, our findings highlight LNC100-S8 as promising nanocarriers for enhancing ICG-based PTT, supporting their potential applications *in vivo* to treat inoperable melanoma and other skin cancers.

References

Abbas, Z. N., Al-Saffar, A. Z., Jasim, S. M., & Sulaiman, G. M. (2023). Comparative analysis between 2D and 3D colorectal cancer culture models for insights into cellular morphological and transcriptomic variations. *Scientific Reports*, *13*(1). https://doi.org/10.1038/s41598-023-45144-w

Abd-El-Azim, H., Tekko, I. A., Ali, A., Ramadan, A., Nafee, N., Khalafallah, N., Rahman, T., McDaid, W., Aly, R. G., Vora, L. K., Bell, S. J., Furlong, F., McCarthy, H. O., & Donnelly, R. F. (2022). Hollow microneedle assisted intradermal delivery of hypericin lipid nanocapsules with light enabled photodynamic therapy against skin cancer. *Journal of Controlled Release*, *348*, 849-869. https://doi.org/10.1016/j.jconrel.2022.06.027

Abdel-Mottaleb, M. M. A., Neumann, D., & Lamprecht, A. (2011). Lipid nanocapsules for dermal application: A comparative study of lipid-based versus polymer-based nanocarriers.

European Journal of Pharmaceutics and Biopharmaceutics, *79*(1), 36-42. https://doi.org/10.1016/j.ejpb.2011.04.009

Andreea Campu, M. F., Frederic Lerouge, Raluca Borlan, Leopold Tie, Dumitrita Rugina, Simion Astilean. (2020). ICG-loaded gold nano-bipyramids with NIR activatable dual PTT-PDT therapeutic potential in melanoma cells. *Colloids and Surfaces B: Biointerfaces*, *194*. https://doi.org/10.1016/j.colsurfb.2020.111213

Arrua, E. C., Hartwig, O., Loretz, B., Murgia, X., Ho, D.-K., Bastiat, G., Lehr, C.-M., & Salomon, C. J. (2023). Formulation of benznidazole-lipid nanocapsules: Drug release, permeability, biocompatibility, and stability studies. *International Journal of Pharmaceutics*, *642*, 123120. https://doi.org/10.1016/j.ijpharm.2023.123120

Béatrice Heurtault, P. S., Brigitte Pech, Jacques-Emile Proust, Jean-Pierre Benoit (2002). A novel phase inversion-based process for the preparation of lipid nanocarriers. *Pharmaceutical research*, *19*(6), 875-880. https://doi.org/10.1023/a:1016121319668

Chen, Q., Xu, L., Liang, C., Wang, C., Peng, R., & Liu, Z. (2016). Photothermal therapy with immune-adjuvant nanoparticles together with checkpoint blockade for effective cancer immunotherapy. *Nature Communications*, *7*(1), 13193. https://doi.org/10.1038/ncomms13193

Cordeiro Lima Fernandes, P., David De Moura, L., Freitas De Lima, F., Henrique Rodrigues Da Silva, G., Isaias Carvalho Souza, R., & De Paula, E. (2021). Lipid nanocapsules loaded with prilocaine and lidocaine and incorporated in gel for topical application. *International Journal of Pharmaceutics*, *602*, 120675. https://doi.org/10.1016/j.ijpharm.2021.120675

Dabholkar, N., Waghule, T., Krishna Rapalli, V., Gorantla, S., Alexander, A., Narayan Saha, R., & Singhvi, G. (2021). Lipid shell lipid nanocapsules as smart generation lipid nanocarriers. *Journal of Molecular Liquids*, *339*, 117145. https://doi.org/10.1016/j.molliq.2021.117145

DeMuth, P. C., Moon, J. J., Suh, H., Hammond, P. T., & Irvine, D. J. (2012). Releasable Layer-by-Layer Assembly of Stabilized Lipid Nanocapsules on Microneedles for Enhanced Transcutaneous Vaccine Delivery. *ACS Nano*, *6*(9), 8041-8051. https://doi.org/10.1021/nn302639r

Drewes, C., De Cristo Soares Alves, A., Hebeda, C., Copetti, I., Sandri, S., Uchiyama, M., Araki, K., Guterres, S., Pohlmann, A., & Farsky, S. (2017). Role of poly(ε-caprolactone) lipid-core nanocapsules on melanoma–neutrophil crosstalk. *International Journal of Nanomedicine*, *Volume 12*, 7153-7163. https://doi.org/10.2147/ijn.s140557

El-Sheridy, N. A., Ramadan, A. A., Eid, A. A., & El-Khordagui, L. K. (2019). Itraconazole lipid nanocapsules gel for dermatological applications: In vitro characteristics and treatment of induced cutaneous candidiasis. *Colloids and Surfaces B: Biointerfaces*, *181*, 623-631. https://doi.org/10.1016/j.colsurfb.2019.05.057

Elmowafy, M., Shalaby, K., Elkomy, M. H., Awad Alsaidan, O., Gomaa, H. A. M., Abdelgawad, M. A., Massoud, D., Salama, A., & El-Say, K. M. (2022). Development and assessment of phospholipid-based luteolin-loaded lipid nanocapsules for skin delivery. *International Journal of Pharmaceutics*, *629*, 122375. https://doi.org/10.1016/j.ijpharm.2022.122375

Filipiak-Duliban, A., Brodaczewska, K., Kajdasz, A., & Kieda, C. (2022). Spheroid Culture Differentially Affects Cancer Cell Sensitivity to Drugs in Melanoma and RCC Models. *International Journal of Molecular Sciences*, *23*(3), 1166. https://www.mdpi.com/1422-0067/23/3/1166

Genina, E. A., Bashkatov, A. N., Simonenko, G. V., Odoevskaya, O. D., Tuchin, V. V., & Altshuler, G. B. (2004). Low-intensity indocyanine-green laser phototherapy of acne vulgaris: Pilot study. *Journal of Biomedical Optics*, *9*(4), 828. https://doi.org/10.1117/1.1756596

Gonçalves, D. P. N., Rodriguez, R. D., Kurth, T., Bray, L. J., Binner, M., Jungnickel, C., Gür, F. N., Poser, S. W., Schmidt, T. L., Zahn, D. R. T., Androutsellis-Theotokis, A., Schlierf, M., & Werner, C. (2017). Enhanced targeting of invasive glioblastoma cells by peptide-functionalized gold nanorods in hydrogel-based 3D cultures. *Acta Biomaterialia*, *58*, 12-25. https://doi.org/10.1016/j.actbio.2017.05.054

Hatahet, T., Morille, M., Hommoss, A., Devoisselle, J. M., Müller, R. H., & Bégu, S. (2018). Liposomes, lipid nanocapsules and smartCrystals®: A comparative study for an effective quercetin delivery to the skin. *International Journal of Pharmaceutics*, *542*(1-2), 176-185. https://doi.org/10.1016/j.ijpharm.2018.03.019

Hatahet, T., Morille, M., Shamseddin, A., Aubert-Pouessel, A., Devoisselle, J. M., & Begu, S. (2017). Dermal quercetin lipid nanocapsules: Influence of the formulation on antioxidant activity and cellular protection against hydrogen peroxide. *Int J Pharm*, *518*(1-2), 167-176. https://doi.org/10.1016/j.ijpharm.2016.12.043

Heurtault, B., Saulnier, P., Pech, B., Proust, J.-E., & Benoit, J.-P. (2002). A novel phase inversion-based process for the preparation of lipid nanocarriers. *Pharmaceutical research*, *19*, 875-880.

Hoarau, D., Delmas, P., David, S., Roux, E., & Leroux, J.-C. (2004). Novel Long-Circulating Lipid Nanocapsules. *Pharmaceutical research*, *21*(10), 1783-1789. https://doi.org/10.1023/b:pham.0000045229.87844.21

Hsu, C.-W., Hsieh, M.-H., Xiao, M.-C., Chou, Y.-H., Wang, T.-H., & Chiang, W.-H. (2020). pH-responsive polymeric micelles self-assembled from benzoic-imine-containing alkyl-modified PEGylated chitosan for delivery of amphiphilic drugs. *International Journal of Biological Macromolecules*, *163*, 1106-1116. https://doi.org/10.1016/j.ijbiomac.2020.07.110

Hureaux, J., Lagarce, F., Gagnadoux, F., Rousselet, M.-C., Moal, V., Urban, T., & Benoit, J.-P. (2010). Toxicological Study and Efficacy of Blank and Paclitaxel-Loaded Lipid Nanocapsules After i.v. Administration in Mice. *Pharmaceutical research*, *27*(3), 421-430. https://doi.org/10.1007/s11095-009-0024-y

Huynh, N. T., Passirani, C., Saulnier, P., & Benoit, J. P. (2009). Lipid nanocapsules: A new platform for nanomedicine. *International Journal of Pharmaceutics*, *379*(2), 201-209. https://doi.org/10.1016/j.ijpharm.2009.04.026

Idlas, P., Lepeltier, E., Jaouen, G., & Passirani, C. (2021). Ferrocifen Loaded Lipid Nanocapsules: A Promising Anticancer Medication against Multidrug Resistant Tumors. *Cancers*, *13*(10), 2291. https://doi.org/10.3390/cancers13102291

Jian, W.-H., Yu, T.-W., Chen, C.-J., Huang, W.-C., Chiu, H.-C., & Chiang, W.-H. (2015). Indocyanine Green-Encapsulated Hybrid Polymeric Nanomicelles for Photothermal Cancer Therapy. *Langmuir*, *31*(22), 6202-6210. https://doi.org/10.1021/acs.langmuir.5b00963

Jung, D., Seung, N. R., Seo, S. B., Park, E. J., & Kim, K. H. (2024). Skin rejuvenation through topical application of indocyanine green with diffractive optical element mode of 785 nm picosecond laser in Asian females. *Journal of Cosmetic Dermatology*, *23*(7), 2411-2419. https://doi.org/10.1111/jocd.16275

Jung, H. S., Verwilst, P., Sharma, A., Shin, J., Sessler, J. L., & Kim, J. S. (2018). Organic molecule-based photothermal agents: an expanding photothermal therapy universe. *Chemical Society Reviews*, *47*(7), 2280-2297.

Kim, D., & Kim, H. (2023). Study on Apoptosis of Squamous Cell Carcinoma Using Photothermal Therapy with Partial Injection of Gold Nanoparticles. *Nanoscale and Microscale Thermophysical Engineering*, *27*(3-4), 135-148. https://doi.org/10.1080/15567265.2023.2220769

Lee, E.-H., Lim, S.-J., & Lee, M.-K. (2019). Chitosan-coated liposomes to stabilize and enhance transdermal delivery of indocyanine green for photodynamic therapy of melanoma. *Carbohydrate Polymers*, *224*, 115143. https://doi.org/10.1016/j.carbpol.2019.115143

Lee, Y. H., Kuo, P. W., Chen, C. J., Sue, C. J., Hsu, Y. F., & Pan, M. C. . (2021). Indocyanine Green-Camptothecin Co-Loaded Perfluorocarbon Double-Layer Nanocomposite: A Versatile Nanotheranostics for Photochemotherapy and FDOT Diagnosis of Breast Cancer. *Pharmaceutics*, *13(9)*. https://doi.org/10.3390/pharmaceutics13091499

Li, W., Zhang, H., Guo, X., Wang, Z., Kong, F., Luo, L., Li, Q., Zhu, C., Yang, J., Lou, Y., Du, Y., & You, J. (2017). Gold Nanospheres-Stabilized Indocyanine Green as a Synchronous Photodynamic–Photothermal Therapy Platform That Inhibits Tumor Growth and Metastasis. *ACS Applied Materials & Interfaces*, *9*(4), 3354-3367. https://doi.org/10.1021/acsami.6b13351

Li, X., Lovell, J. F., Yoon, J., & Chen, X. (2020). Clinical development and potential of photothermal and photodynamic therapies for cancer. *Nature Reviews Clinical Oncology*, *17*(11), 657-674. https://doi.org/10.1038/s41571-020-0410-2

Liang, P., Mao, L., Dong, Y., Zhao, Z., Sun, Q., Mazhar, M., Ma, Y., Yang, S., & Ren, W. (2021). Design and Application of Near-Infrared Nanomaterial-Liposome Hybrid Nanocarriers for Cancer Photothermal Therapy. *Pharmaceutics*, *13*(12), 2070. https://doi.org/10.3390/pharmaceutics13122070

Lopes, J., Rodrigues, C. M. P., Gaspar, M. M., & Reis, C. P. (2022). How to Treat Melanoma? The Current Status of Innovative Nanotechnological Strategies and the Role of Minimally Invasive Approaches like PTT and PDT. *Pharmaceutics*, *14*(9), 1817. https://doi.org/10.3390/pharmaceutics14091817

Maupas, C., Moulari, B., Béduneau, A., Lamprecht, A., & Pellequer, Y. (2011). Surfactant dependent toxicity of lipid nanocapsules in HaCaT cells. *International Journal of Pharmaceutics*, *411*(1-2), 136-141.

Mazzarino, L., Dora, C. L., Bellettini, I. C., Minatti, E., Cardoso, S. G., & Lemos-Senna, E. (2010). Curcumin-loaded polymeric and lipid nanocapsules: preparation, characterization and chemical stability evaluation. *Lat. Am. J. Pharm*, *29*(6), 933-940.

Morille, M., Passirani, C., Dufort, S., Bastiat, G., Pitard, B., Coll, J.-L., & Benoit, J.-P. (2011). Tumor transfection after systemic injection of DNA lipid nanocapsules. *Biomaterials*, *32*(9), 2327-2333. https://doi.org/10.1016/j.biomaterials.2010.11.063

Mu, M., Liang, X., Chuan, D., Zhao, S., Yu, W., Fan, R., Tong, A., Zhao, N., Han, B., & Guo, G. (2021). Chitosan coated pH-responsive metal-polyphenol delivery platform for melanoma chemotherapy. *Carbohydrate Polymers*, *264*, 118000. https://doi.org/10.1016/j.carbpol.2021.118000

Muraleedharan, S., & Tripathy, K. (2023). *Indocyanine Green (ICG) Angiography*. StatPearls

Publishing, Treasure Island (FL). http://europepmc.org/abstract/MED/35593804
http://europepmc.org/books/NBK580479
https://www.ncbi.nlm.nih.gov/books/NBK580479

Nguyen, H. T. P., Munnier, E., Perse, X., Vial, F., Yvergnaux, F., Perrier, T., Soucé, M., & Chourpa, I. (2016). Qualitative and Quantitative Study of the Potential of Lipid Nanocapsules of One Hundred Twenty Nanometers for the Topical Administration of Hydrophobic Molecules. *JOURNAL OF PHARMACEUTICAL SCIENCES*, *105*(10), 3191-3198. https://doi.org/10.1016/j.xphs.2016.06.025

Ntziachristos, V., Yodh, A. G., Schnall, M., & Chance, B. (2000). Concurrent MRI and diffuse optical tomography of breast after indocyanine green enhancement. *Proceedings of the National Academy of Sciences*, *97*(6), 2767-2772. https://doi.org/10.1073/pnas.040570597

Pereira Gomes, I., Aparecida Duarte, J., Chaves Maia, A. L., Rubello, D., Townsend, D. M., Branco De Barros, A. L., & Leite, E. A. (2019). Thermosensitive Nanosystems Associated with Hyperthermia for Cancer Treatment. *Pharmaceuticals*, *12*(4), 171. https://doi.org/10.3390/ph12040171

Sevieri, M., Silva, F., Bonizzi, A., Sitia, L., Truffi, M., Mazzucchelli, S., & Corsi, F. (2020). Indocyanine Green Nanoparticles: Are They Compelling for Cancer Treatment? *Frontiers in chemistry*, *8*. https://doi.org/10.3389/fchem.2020.00535

Sharma, K., Dey, S., Karmakar, R., & Rengan, A. K. (2024). A comprehensive review of 3D cancer models for drug screening and translational research. *Cancer Innovation*, *3*(1). https://doi.org/10.1002/cai2.102

Shemesh, C. S., Hardy, C. W., Yu, D. S., Fernandez, B., & Zhang, H. (2014). Indocyanine green loaded liposome nanocarriers for photodynamic therapy using human triple negative breast cancer cells. *Photodiagnosis and Photodynamic Therapy*, *11*(2), 193-203. https://doi.org/10.1016/j.pdpdt.2014.02.001

Shirata, C., Kaneko, J., Inagaki, Y., Kokudo, T., Sato, M., Kiritani, S., Akamatsu, N., Arita, J., Sakamoto, Y., Hasegawa, K., & Kokudo, N. (2017). Near-infrared photothermal/photodynamic therapy with indocyanine green induces apoptosis of hepatocellular carcinoma cells through oxidative stress. *Scientific Reports*, *7*(1). https://doi.org/10.1038/s41598-017-14401-0

Shiyi Zhou, D. L., Chaebin Lee, and Jin Xie. (2020). Nanoparticle Phototherapy in the Era of Cancer Immunotherapy. *Trends Chem*, *Dec;2(12)*, 1082-1095. https://doi.org/10.1016/j.trechm.2020.09.008

Simon, L., Lapinte, V., Lionnard, L., Marcotte, N., Morille, M., Aouacheria, A., Kissa, K., Devoisselle, J. M., & Bégu, S. (2020). Polyoxazolines based lipid nanocapsules for topical delivery of antioxidants. *International Journal of Pharmaceutics*, *579*, 119126. https://doi.org/10.1016/j.ijpharm.2020.119126

Teng, C. W., Huang, V., Arguelles, G. R., Zhou, C., Cho, S. S., Harmsen, S., & Lee, J. Y. K. (2021). Applications of indocyanine green in brain tumor surgery: review of clinical evidence and emerging technologies. *Neurosurgical Focus*, *50*(1), E4. https://doi.org/10.3171/2020.10.focus20782

Terroso, T., Külkamp, I. C., Jornada, D. S., Pohlmann, A. R., & Guterres, S. S. (2009). Development of semi-solid cosmetic formulations containing coenzyme Q10-loaded nanocapsules. *Lat Am J Pharm*, *28*(6), 819-826.

Topaloğlu, N., Kadıköylü, G., Onak, G., & Karaman, O. (2020). The effect of indocyanine green-based photodynamic therapy on healthy fibroblast and keratinocyte cells. *Photodiagnosis and Photodynamic Therapy*, *31*, 101891. https://doi.org/10.1016/j.pdpdt.2020.101891

Totonchy, M., & Leffell, D. (2017). Emerging concepts and recent advances in basal cell carcinoma. *F1000Research*, *6*, 2085. https://doi.org/10.12688/f1000research.11314.1

Wu, S., Hatahet, T., & Al-Jamal, W. (2025). Span80 surfactant improves lipid nanocapsules biocompatibility and increases their cellular uptake in the B16F10 melanoma cell line. *International Journal of Pharmaceutics*, *In press*.

Yaseen, M. A., Yu, J., Wong, M. S., & Anvari, B. (2007). Laser-Induced Heating of Dextran-Coated Mesocapsules Containing Indocyanine Green. *Biotechnology Progress*, *23*(6), 1431-1440. https://doi.org/10.1021/bp0701618

Yoon, H.-J., Lee, H.-S., Lim, J.-Y., & Park, J.-H. (2017). Liposomal Indocyanine Green for Enhanced Photothermal Therapy. *ACS Applied Materials & Interfaces*, *9*(7), 5683-5691. https://doi.org/10.1021/acsami.6b16801

Yorozu, K., Kaibori, M., Kimura, S., Ichikawa, M., Matsui, K., Kaneshige, S., Kobayashi, M., Jimbo, D., Torikai, Y., Fukuzawa, Y., & Okamoto, Y. (2022). Experience with Photodynamic Therapy Using Indocyanine Green Liposomes for Refractory Cancer. *Journal of Personalized Medicine*, *12*(7), 1039. https://doi.org/10.3390/jpm12071039

Zhao, P., Zheng, M., Yue, C., Luo, Z., Gong, P., Gao, G., Sheng, Z., Zheng, C., & Cai, L. (2014). Improving drug accumulation and photothermal efficacy in tumor depending on size of ICG loaded lipid-polymer nanoparticles. *Biomaterials*, *35*(23), 6037-6046. https://doi.org/10.1016/j.biomaterials.2014.04.019

Zheng, X., Xing, D., Zhou, F., Wu, B., & Chen, W. R. (2011). Indocyanine Green-Containing Nanostructure as Near Infrared Dual-Functional Targeting Probes for Optical Imaging and Photothermal Therapy. *Molecular Pharmaceutics*, *8*(2), 447-456. https://doi.org/10.1021/mp100301t

Zheng, X., Zhou, F., Wu, B., Chen, W. R., & Xing, D. (2012). Enhanced Tumor Treatment Using Biofunctional Indocyanine Green-Containing Nanostructure by Intratumoral or Intravenous Injection. *Molecular Pharmaceutics*, *9*(3), 514-522. https://doi.org/10.1021/mp200526m

Zhi, D., Yang, T., O'Hagan, J., Zhang, S., & Donnelly, R. F. (2020). Photothermal therapy. *Journal of Controlled Release*, *325*, 52-71. https://doi.org/10.1016/j.jconrel.2020.06.032

Zuchowska, A., Jastrzebska, E., Chudy, M., Dybko, A., & Brzozka, Z. (2017). 3D lung spheroid cultures for evaluation of photodynamic therapy (PDT) procedures in microfluidic Lab-on-a-Chip system. *Analytica Chimica Acta*, *990*, 110-120. https://doi.org/10.1016/j.aca.2017.07.009